PNAS RESEARCH ARTICLE | PLANT BIOLOGY

A change in the cell wall status initiates the elimination of the nucellus in *Arabidopsis*

Miryam Iannaccone[a,1], Wenjia Xu[a,1,2], Dennys-Marcela Gomez-Paez[a], Sandrine Choinard[a], Elisa Maricchiolo[b], Alexis Peaucelle[a], Aline Voxeur[a], Kalina Tamara Haas[a], Catherine Lapierre[a], Jose M. Jiménez-Gómez[c], Andrea Pompa[b], and Enrico Magnani[a,2]

Edited by R. Scott Poethig, University of Pennsylvania, Philadelphia, PA; received June 17, 2025; accepted February 13, 2026

The evolution of the seed habit can be traced back to a change in the cell fate of the nucellus, the sporophytic tissue responsible for female meiosis. Seeds arose when the nucellus retained the female spores instead of releasing them into the environment. As a consequence, the nucellus was partially eliminated to accommodate the growth of the female gametophyte inside the sporophyte. With the evolution of angiosperm seeds, the process of nucellus elimination was requisitioned to allow the growth of the endosperm, the fertilization product devoted to storing nutrients that are at the foundation of the human diet. Cell elimination differs from most known cell death programs as it leads to the apparent dismantling of the cell wall. Here, we show that nucellus elimination in *Arabidopsis* is initiated by demethylesterification and subsequent lysis of the pectic polysaccharides in the cell wall. This process exposes other cell wall components to possible further degradation and precedes a cell death program that leads to nuclear DNA fragmentation. Both pathways are regulated by TRANSPARENT TESTA 16, a MADS-domain transcription factor that evolved with seed plants. Our results highlight a convergence in the structure and function of extracellular polysaccharides in animals and plants and emphasize their crucial contribution to the development of multicellular organisms.

fertilization | seed | pectins | cell elimination

Significance

Seeds evolved when plants retained the female spores inside the parent tissue. The growth of the spores was accommodated by removing part of the nucellus, the maternal tissue responsible for female meiosis. Here, we demonstrate that modification of galacturonic acid polymers in the cell wall leads to nucellus cell death and eventual elimination. This work highlights the crucial contribution of extracellular polysaccharides to the development of multicellular organisms.

The nucellus (also referred to as megasporangium) is the plant tissue undergoing female meiosis. Within the nucellus, a single subepidermal cell differentiates into the megaspore mother cell, the cell that executes meiosis to form megaspores, effectively serving as the germline niche for female reproductive development (1). In heterosporous nonseed plants, the nucellus sporophytic tissue releases female spores in the environment, thus separating the female gametophyte from the sporophyte (2). The evolution of the seed habit is marked, instead, by the retention of the female spores in the nucellus and the dispersal of the zygotic embryo, the next sporophytic generation (3, 4). Seed plants evolved, therefore, the ability to eliminate part of the nucellus tissue in order to accommodate the growth of the female gametophyte inside the sporophyte. With the evolution of angiosperm seeds, the nucellus is further consumed by the endosperm, the fertilization product responsible for storing nutrients and nourishing the embryo (4–7). Such changes in the cell fate of the nucellus allowed a "revolution" in human society, as seeds are the foundation of agriculture and human diet.

Differences have been observed in the level of nucellus elimination among different plant species (5). In endospermic seeds, such as those of cereals and *Arabidopsis*, the nucellus occupies most of the ovule volume at anthesis but is largely eliminated after fertilization. The few nucellar cell layers that persist—typically at the periphery and along the vascular trace—remain metabolically active and contribute to nutrient transfer toward the developing endosperm and embryo. By contrast, perispermic seeds display a large central nucellus (perisperm) that grows to become the main storage tissue along a minute endosperm. Seeds with architectures that fall between these two extremes have also been documented. For example, a retard in the elimination of the nucellus is a hallmark of coffee grains (8, 9) while nucellus and endosperm coexist and display a similar volume in *Acorus calamus* seeds (10).

The signaling pathway leading to the elimination of the nucellus has been elucidated in *Arabidopsis* seeds. A first round of cell elimination is initiated in the ovule during the growth of the female gametophyte and is marked by a maximum auxin response (11–13). After fertilization, the endosperm triggers the elimination of around ten cell layers of the nucellus (hereafter referred to as "transient nucellus," TN) (Fig. 1 *A* and *B*) (5, 14, 15). The AGAMOUS LIKE 62 (AGL62) MADS-domain transcription factor is hypothesized

Author affiliations: [a]Institut Jean-Pierre Bourgin, Institut National de Rrecherche pour l'Agriculture, l'Alimentation et l'Environnement, AgroParisTech, CNRS, University of Paris-Saclay, Versailles Cedex 78026, France; [b]Section of Biological and Biotechnological Sciences, Department of Biomolecular Sciences, University of Urbino Carlo Bo, Urbino 61029, Italy; and [c]Centro de Biotecnología y Genómica de Plantas, UPM-INIA-CSIC, Campus de Montegancedo, Madrid 28223, Spain

Author contributions: W.X. and E.M. designed research; M.I., W.X., D.-M.G.-P., S.C., E.M., A. Peaucelle, A.V., K.T.H., C.L., J.M.J.-G., and E.M. performed research; M.I., W.X., D.-M.G.-P., S.C., E.M., A. Peaucelle, A.V., K.T.H., C.L., J.M.J.-G., A. Pompa, and E.M. analyzed data; and E.M. wrote the paper.

The authors declare no competing interest.

This article is a PNAS Direct Submission.

[1]M.I. and W.X. contributed equally to this work.

[2]To whom correspondence may be addressed. Email: wenjia.xu@inrae.fr or enrico.magnani@inrae.fr.

This article contains supporting information online at https://www.pnas.org/lookup/suppl/doi:10.1073/pnas.2515702123/-/DCSupplemental.

Published May 5, 2026.

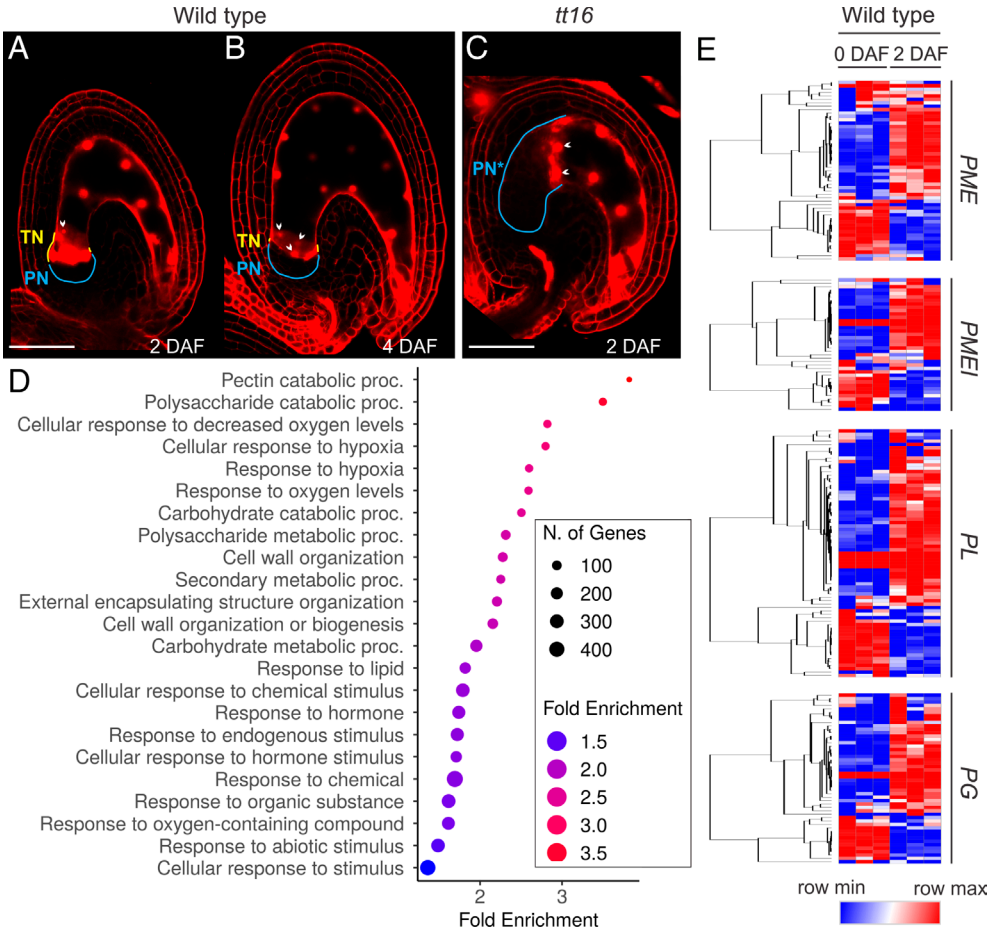

Fig. 1. Transcriptional changes in pectin modifier genes induced by fertilization. (*A–C*) Propidium iodide fluorescence images of whole mount wild-type (WT) and *tt16* seeds. DAF, days after flowering; TN, transient nucellus (yellow); PN, persistent nucellus (cyan); PN*, PN + TN not eliminated (cyan). White arrowheads indicate endosperm nuclei close to the nucellus. (Scale bar, 50 μm.) (*D*) Enriched GO terms for genes differentially expressed across fertilization (log2 fold change threshold ± 1) and detected in the WT nucellus/chalaza domain of the seed. (*E*) Heatmaps showing the expression across fertilization of *PECTIN METHYLESTERASE* (*PME*), *PECTIN METHYLESTERASE INHIBITOR* (*PMEI*), *PECTATE LYASE* (*PL*), and *POLYGALACTURONASE* (*PG*) genes detected in the WT nucellus/chalaza domain of the seed. Three replicates per time point are shown.

to send a signal from the endosperm to relieve the repressive action mediated by FERTILIZATION INDEPENDENT SEED (FIS) Polycomb group (PcG) proteins on TN elimination. Downstream of FIS PcG proteins, the TRANSPARENT TESTA 16 (TT16) MADS-domain transcription factor promotes the elimination of the TN, a function shown to be partially conserved in other species (6, 7, 16, 17). Finally, around four proximal cell layers of the nucellus (hereafter referred to as "persistent nucellus," PN) (Fig. 1 *A* and *B*) survive throughout seed development and play a role in sugar transport (5, 14, 15).

Compared to most other cell death programs, which preserve the cell wall, cell elimination is characterized by the complete dismantling of unwanted cells, leaving no easily detectable cell corpse (18, 19). Images of the *Arabidopsis* TN, obtained by transmission electron microscopy, displayed cell walls consumed to the breaking point and the release of intracellular material in the apoplastic space (14). While this process appears to be conserved among different endospermic seeds (5, 18), cell wall elimination in the TN has never been investigated beyond its morphological characterization. Primary cell walls are mostly composed of structural proteins and three families of polymers: cellulose, hemicelluloses, and pectins (20, 21). Cellulose accounts for 30 to 40% of the wall mass and constitutes the main backbone of the cell wall. Hemicelluloses are a diverse family of polymers, including xyloglucans, xylans, and mannans, that strengthen the cell wall by interacting with cellulose. Finally, pectins are heterogeneous polysaccharides rich in galacturonic acid accounting for up to 35% of primary cell walls. To characterize how the cell walls of the TN are eliminated, we conducted an in silico analysis of transcriptomic data across fertilization in *Arabidopsis* (a model for nucellus elimination in endospermic seeds), which pointed toward a change in pectin metabolism. A combination of immunolabeling, genetic and biochemical analyses showed that the pectic polysaccharide homogalacturonan (HG) is demethylesterified and eventually degraded by pectate lyases in the TN, at the onset of cell elimination. In addition, histochemical studies revealed that HG degradation exposes cellulose to possible further degradation. We found that HG demethylesterification is promptly followed by DNA fragmentation, a hallmark of cell death, and that both processes are promoted by TT16. The *tt16* mutation also induced the lignification of the nucellus cell walls, a characteristic feature of the hypostasis in monocotyledons. Finally, we demonstrated that inhibition of HG demethylesterification arrests TN elimination, thus indicating that modulation of the pectin status influences nucellus cell fate.

Results

Fertilization Induces the Expression of Pectin Modifier Genes in the Nucellus. In *Arabidopsis*, the elimination of the transient nucellus (TN, Fig. 1 *A* and *B*) is characterized by the apparent

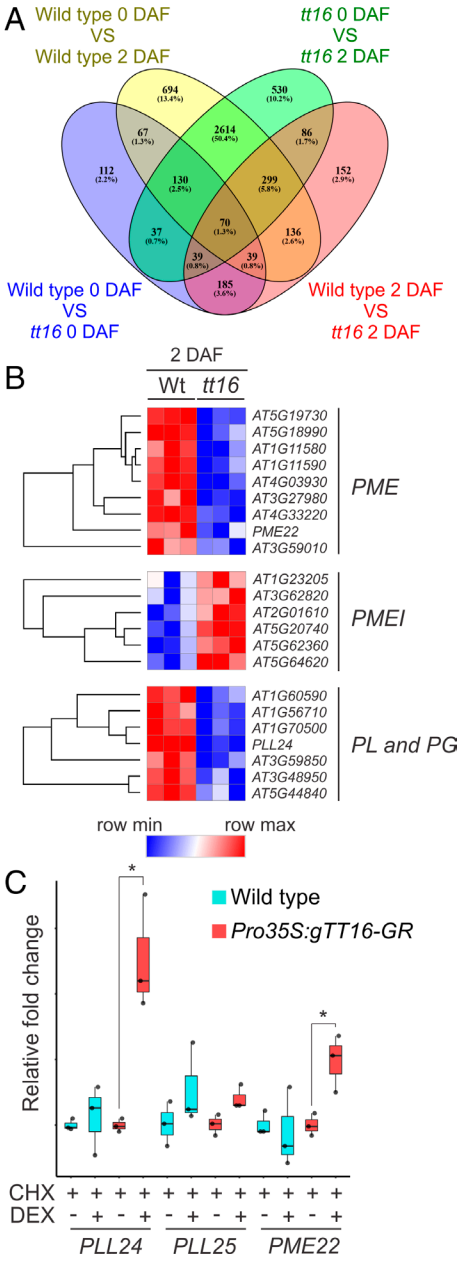

Fig. 2. TT16 regulates pectin modifier genes. (*A*) Venn diagram of number of differentially expressed genes (DEGs, log2 fold change threshold ± 1) across time points (0 and 2 DAF) and genotypes (WT and *tt16*). The proportion of DEGs in each subgroup, relative to the total number of DEGs, is indicated in percentage values. (*B*) Heatmaps showing the expression of *PECTIN METHYLESTERASE* (*PME*), *PECTATE LYASE* (*PL*), and *POLYGALACTURONASE* (*PG*) genes down-regulated and *PECTIN METHYLESTERASE INHIBITORS* (*PMEI*) genes up-regulated in the *tt16* mutant at 2 DAF, when compared to the WT. All pectin modifier genes shown are expressed in the WT nucellus/chalaza domain of the seed. Three replicates per genotype are shown. (*C*) Quantitative RT-PCR analyses of *PLL24*, *PLL25*, and *PME22* expression in WT and Pro*35S:gTT16-GR* seeds (2 DAF) treated with cycloheximide (CHX, plus sign) and dexamethasone (DEX, plus sign) or mock solution (minus sign). Expression levels were normalized to the *UBIQUITIN9* expression and were averaged from three independent biological samples. Values of mock treated inflorescences are arbitrarily set to one. Asterisks indicate statistically significant differences (Student's *t* test, $P < 0.05$). Error bars indicate SD.

clearance of the entire cell corpses, including the cell walls, in response to fertilization (14). To investigate this unique process, we conducted a transcriptomic analysis aimed at identifying cell wall-related genes expressed in the nucellus in response to fertilization. We sorted genes differentially expressed (DEGs, log2 fold change threshold ± 1) in siliques between 0 d after flowering (0 DAF, right before nucellus elimination begins) and 2 DAF (during the process of nucellus elimination) (Dataset S1 and *SI Appendix*, Fig. S1). Among these DEGs, we selected genes expressed in the nucellus/chalaza domain of seeds at the preglobular embryo stage, according to transcriptomic data obtained by laser capture microdissection (average signal > 10) (22). Finally, we conducted a Gene Ontology (GO) analysis and detected significant enrichments in GO annotations for "pectin catabolic process" and "cell wall organization" (Fig. 1*D*). In particular, a relatively high number of *PECTIN METHYLESTERASE* (*PME*), *PECTIN METHYLESTERASE INHIBITOR* (*PMEI*), *PECTATE LYASE* (*PL*), and *POLYGALACTURONASE* (*PG*) genes were differentially expressed across fertilization (Fig. 1*E* and Dataset S1). We obtained similar results by applying the same analysis to transcriptomic data generated by Figueiredo et al. (23) with unfertilized ovules at 4 d after emasculation, in which the nucellus is not eliminated (14), and seeds at 2 d after pollination (corresponding to three DAF). Among genes up-regulated after fertilization and expressed in the chalaza-nucellus tissue, we detected significant enrichments in GO annotations for "pectin metabolic process" (*P*-value 7.17E-04) and "cell wall modification" (*P*-value 9.76E-04) (Dataset S2).

The process of nucellus elimination is promoted by the TT16 MADS-domain transcription factor (14). We therefore analyzed *tt16* mutant seeds, which display an almost intact nucellus (referred to as PN* because it is made of PN and TN not eliminated) where only a few distal cells degenerate (Fig. 1*C*). We conducted transcriptomic analyses of *tt16* siliques at 0 and 2 DAF and compared them to the data obtained in the WT (Dataset S1 and *SI Appendix*, Fig. S1, and Fig. 2*A*). We observed a number of pectin modifier genes (*PMEs*, *PMEIs*, *PLs*, and *PGs*) expressed in the nucellus/chalaza domain of the seed (22) being regulated by TT16 at 2 DAF (Fig. 2*B*). To confirm our transcriptomics results, we analyzed the transcriptional response of pectin modifier genes to an inducible TT16 transcription factor fused to the rat glucocorticoid receptor (GR) under the control of the constitutive cauliflower mosaic virus *35S* promoter (*Pro35S:gTT16-GR*), previously described (14). Dexamethasone (DEX) treatment releases the GR-transcription factor chimeric protein from a cytoplasmic HEAT SHOCK PROTEIN90 complex that prevents its nuclear translocation and therefore its functionality (24). To prevent indirect transcriptional effects of the inducible TT16-GR protein, we infiltrated seeds with cycloheximide, an inhibitor of protein synthesis. Furthermore, we conducted an identical experiment with WT seeds to discount for the unspecific effect of DEX. Finally, we measured transcripts of pectin modifier genes by quantitative RT-PCR on independent samples. The expression of *PECTATE LYASE LIKE 24* (*PLL24*) and *PME22*, which was down-regulated in *tt16* seeds (Fig. 2*B*), did not change after DEX treatment in WT seeds but was significantly up-regulated by TT16-GR induction (Fig. 2*C*). By contrast, the expression of *PLL25*, the closest paralogue of *PLL24* (25), was not affected by either the *tt16* mutation or TT16-GR induction (Fig. 2*C*). Overall, these data suggest that *PLL24* and *PME22* are immediate targets of TT16.

It is generally agreed that homogalacturonan (HG), the most abundant pectin subtype in plant cell walls, is synthesized as a highly methylesterified polymer (26). Demethylesterification of HG by PMEs, a process inhibited by PMEIs, can lead to its degradation by PLs and PGs and influence cell wall integrity (27), thus being a primary suspect in the elimination of the nucellus and therefore the focus of our investigation.

Pectin Demethylesterification and Degradation Mark the Onset of Nucellus Elimination. To test if HG in the TN cell walls is demethylesterified and degraded, we stained whole mount seeds

with propidium iodide (PI), a dye that binds HG carboxyl residues and nucleic acids (Fig. 1 *A* and *B*) (28). PI fluorescence in the cell wall has been shown to increase in the presence of PMEs, which create more binding sites, and decrease in the presence of PLs, which digest HGs (28). To identify the nucellus, we used the inner integument 1, the pigment strand and the endosperm as morphological markers, as previously described (14). PI fluorescence was visible throughout the nucellus at 0 DAF (*SI Appendix*, Fig. S1) and as amorphous signal in the TN at 2 DAF, during the process of cell elimination. The signal in the TN almost completely disappeared at 4 DAF after its degradation (Fig. 1 *A* and *B*). PI also stained endosperm nuclei, recognizable by their round shape (Fig. 1 *A* and *B*). By contrast, we detected a relatively lower PI signal in the PN of seeds at both time points tested (Fig. 1 *A* and *B* and *SI Appendix*, Fig. S1) and in the PN* of *tt16* seeds at 2 DAF (Fig. 1*C* and *SI Appendix*, Fig. S1). These data suggest that HG is demethylesterified (at 2 DAF) and degraded (at 4 DAF) in the WT TN whereas it remains highly methylesterified in the WT PN and *tt16* PN*.

To further test this hypothesis, we conducted immunolabeling studies using 2F4 and LM20 antibodies, which are specific for low and high methylesterified pectins, respectively (29, 30). During the first 4 DAF, we detected a higher 2F4 signal in the TN nucellus, when compared to the PN (Fig. 3 *A–C* and *SI Appendix*, Fig. S2). This was true even at 1 DAF (Fig. 3*A*), before any morphological marker of nucellus elimination is visible. To precisely analyze the pattern of HG methylesterification, we quantified the fluorescent signal of the 2F4 and LM20 antibodies at 2 DAF and observed a decrease in the relative HG methylesterification status along the proximal–distal axis of the nucellus (Fig. 3 *E* and *F*, *Materials and Methods*). In line with these results, the entire nucellus of *tt16* seeds at 2 DAF displayed relatively high-methylesterified HG (Fig. 3 *D–F*), when compared to the WT TN (Fig. 3 *B, E,* and *F*). Overall, these results indicate that HG demethylesterification is a hallmark of the TN and is promoted by TT16.

To determine if demethylesterified HG in the TN is targeted by pectin-degrading enzymes, we tested our samples with the carbohydrate binding module 3 (CBM3) probe, which binds crystalline cellulose in cells actively depositing cellulose or characterized by a relatively low abundance of pectins (31, 32). The cellulose sites bound by CBM3 are indeed masked by pectins, thus making CBM3 an inverse pectin marker (31). In support of the hypothesis of pectin degradation, we detected CBM3 fluorescence in the TN of seeds at 2 and 4 DAF, in proximity to 2F4 signal (Fig. 3 *B* and *C* and *SI Appendix*, Fig. S2). By contrast, the TN of seeds at 1 DAF displayed 2F4 but not CBM3 fluorescence, suggesting that HG demethylesterification precedes its digestion (Fig. 3*A*). Consistently, the WT PN and *tt16* PN* did not show CBM3 fluorescence (Fig. 3 *A–D*).

To confirm if pectin is digested in the TN, we characterized the localization of the PLL24 enzyme, whose expression was up-regulated in response to fertilization (Fig. 1*E* and Dataset S1), down-regulated in the *tt16* mutant (Fig. 2*B*) and up-regulated by

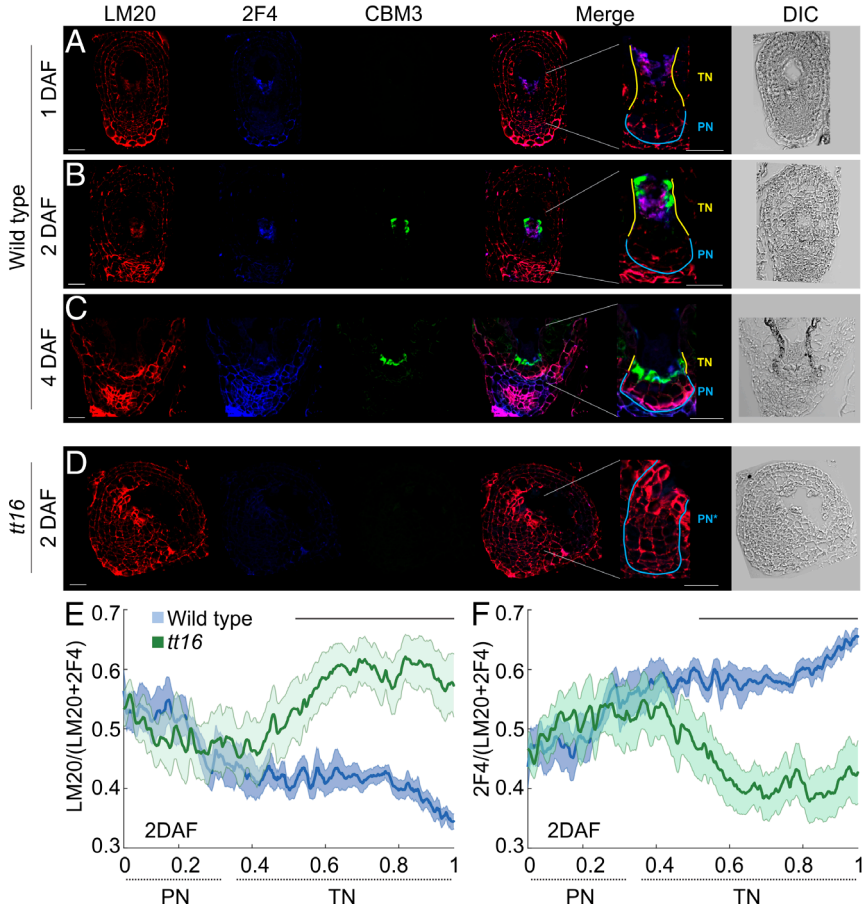

Fig. 3. Pectin methylesterification status in the nucellus. (*A–D*) Triple labeling of WT and *tt16* seed sections with LM20 (specific for high methylesterified pectins, in red) and 2F4 (specific for low methylesterified pectins, in blue) antibodies and the CBM3 (specific for crystalline cellulose, in green) probe. DIC, differential interference contrast image; DAF, days after flowering; TN, transient nucellus (yellow); PN, persistent nucellus (cyan); PN*, PN + TN not eliminated (cyan). (Scale bar, 20 μm.) (*E* and *F*) Mean relative fluorescent signal of LM20 and 2F4 antibodies along the WT and *tt16* nucellus proximal–distal axis (*Materials and Methods*). Lines at the top of the graph indicate regions of statistically significant difference between WT and *tt16* (Wilcoxon test, $P < 0.05$). Error bars indicate SE.

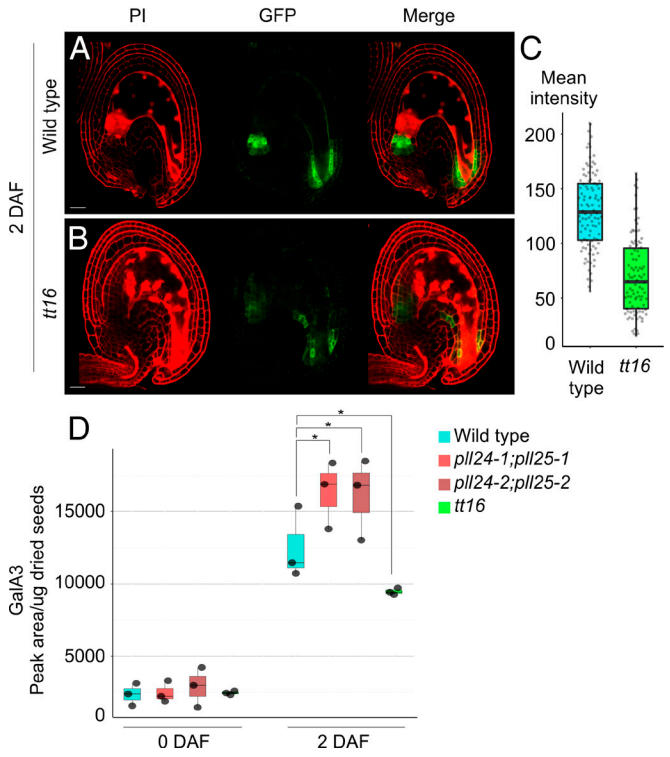

Fig. 4. Pectin degradation in the nucellus. (*A* and *B*) Propidium iodide (PI, in red) and GFP (in green) fluorescence images of whole mount *ProPLL24:PLL24-GFP* WT and *tt16* seeds. (Scale bar, 20 μm.) (*C*) Quantification of GFP fluorescence intensity in the nucellus of *ProPLL24:PLL24-GFP* WT and *tt16* seeds. (*D*) Profiling of the 3-residue galacturonic acid oligomer (GalA3) in WT, *pll,* and *tt16* ovules and seeds. Asterisks indicate statistically significant difference between WT and mutant lines (Student's *t* test, $P < 0.05$). Error bars indicate SD. DAF, days after flowering.

TT16-GR induction (Fig. 2*C*). In line with transcriptomic data obtained by laser capture microdissection of the seed nucellus/chalaza area (22), the *PLL24* promoter and genomic region drove expression of the GREEN FLUORESCENT PROTEIN (*ProPLL24:PLL24-GFP*) in the nucellus of seeds at 2 DAF (Fig. 4*A*). *tt16* seeds displayed PLL24-GFP fluorescence in the nucellus (Fig. 4*B*), albeit less than the WT (Fig. 4*C*) as suggested by our transcriptional analyses (Fig. 2 *B* and *C*). Since we failed to produce the PLL24 protein to test its enzymatic activity, we homology modeled its 3D structure and compared it with previously resolved ones. PLL24 exhibited significant structural conservation with pectate lyases from the Protein Data Bank, with the highest similarity observed to Ply1 from *Juniperus ashei* (E-value 1.38e-33, 1.70 Å, *SI Appendix*, Fig. S3) (33). Notably, the residues critical for Ca^{2+} binding, required for enzymatic activity, and the enzyme's active center are identical in PLL24 and Ply1 (*SI Appendix*, Fig. S3). This result suggests that the HG degrading machinery is present during nucellus elimination.

To challenge our model, we analyzed the HG status of two independent *pll24;pll25* double mutant lines. *PLL25* is the closest paralogue of *PLL24* (25) and its expression is up-regulated after fertilization (Fig. 1*E* and Dataset S1) and localized in the seed nucellus/chalaza domain (22), despite not being an immediate target of TT16 (Fig. 2*C*). *pll24;pll25* seeds appeared indistinguishable from WT ones, when imaged at the confocal microscope (*SI Appendix*, Fig. S2). Furthermore, immunolabeling analyses detected 2F4 and CBM3 signal in the TN of *pll24;pll25* seeds 2 DAF (*SI Appendix*, Fig. S2), as observed in the WT (Fig. 3*B*), probably due to redundancy with other PLL enzymes (25). To more precisely characterize the mutant, we quantified the amount of HG oligomers resulting from the digestion of WT and *pll24;25* mutant cell walls with an endo-polygalacturonase, which hydrolyzes low and nonmethylesterified HGs, using a mass spectrometry sensitive analytical method based on the separation of oligosaccharides combined with accurate determination of their sizes and methylesterification patterns (34, 35). In ovules at 0 DAF, we did not detect any statically significant difference between WT and *pll24;25* mutant samples (Fig. 4*D*). By contrast, digestion of *pll24;pll25* seeds at 2 DAF released significantly more 3-residue galacturonic acid oligomer (GalA3), indicating a higher content of digestible HG compared to the WT (Fig. 4*D*). In accordance with this result, we detected a lower content of GalA3, and therefore digestible HG, in *tt16* mutant seeds 2 DAF, when compared to the WT (Fig. 4*D*). Overall, these data indicate that PLL24 and PLL25 actively digest low-methylesterified HG in response to fertilization.

Pectin Demethylesterification Is Necessary for Nucellus Elimination. To test if HG demethylesterification is necessary to trigger cell elimination, we induced the overexpression of the *PECTIN METHYL ESTERASE INHIBITOR 3* (*PMEI3*) gene, which is known to inhibit PME activity and block HG demethylesterification in *Arabidopsis* (36, 37). To this end, we employed an ethanol-inducible system based on the constitutive *35S* promoter (*iPMEI3-OX*) and overexpressed the *β-glucuronidase* (*GUS*) gene as control *(iGUS-OX)* (36). GUS staining analyses confirmed that this system induced the expression in the nucellus (*SI Appendix*, Fig. S4). At 4 DAF, 63% of *iPMEI3-OX* seeds displayed an enlarged endosperm (Fig. 5*B* and *SI Appendix*, Fig. S5) but did not undergo TN elimination (Fig. 5*B*), similar to *tt16* seeds (Fig. 5*D*) (14). By contrast, the TN of all *iGUS-OX* seeds analyzed was almost completely eliminated (Fig. 5*A*) as in the WT (Fig. 5*C*). As expected, immunolabeling analyses revealed relatively high HG methylesterification in the nucellus of *iPMEI3-OX* seeds and failed to detect CBM3 signal (*SI Appendix*, Fig. S2). In line with this result, we obtained a lower content of GalA3, and therefore digestible HG, in *iPMEI3-OX* seeds when compared to *iGUS-OX* (*SI Appendix*, Fig. S4). Finally, we confirmed our results by inducing the overexpression of a different *PMEI* using an estrogen-inducible system. Seeds overexpressing *PMEI5* (*iPMEI5-OX*) (38) displayed an almost intact nucellus when compared to the WT (*SI Appendix*, Fig. S4). Altogether, these data demonstrate that HG demethylesterification is necessary for the elimination of the TN.

Nuclear DNA Fragmentation Follows Pectin Demethylesterification in the Transient Nucellus. To determine if a cell death program works alongside the breakdown of the cell wall, we tested the TN for nuclear DNA fragmentation, a hallmark of programmed cell death, by terminal deoxynucleotidyl transferase dUTP nick end labeling (TUNEL) (39, 40). We started to observe TUNEL signal at 2 DAF in the most distal cells of the TN (Fig. 6 *A* and *B*), when compared to positive and negative controls (*SI Appendix*, Fig. S6). The signal disappeared in seeds at 4 DAF, where only the PN was visible (Fig. 6*C*). By contrast, we detected a faint signal in only a few distal cells of the *tt16* and *iPMEI3-OX* nucellus at 2 DAF (Fig. 6 *D* and *E*). Finally, TUNEL signal in the *pll24;pll25* TN was comparable to the WT (Fig. 6*F*). These results demonstrate that nuclear DNA fragmentation follows HG demethylesterification and works alongside HG degradation toward the complete elimination of the TN.

TT16 Represses the Lignification of the Transient Nucellus. In a number of monocotyledons, the persistent nucellus in the chalazal region lignifies, forming the so-called hypostase (5, 41). The hypostase is thought to mechanically prevent the growth of

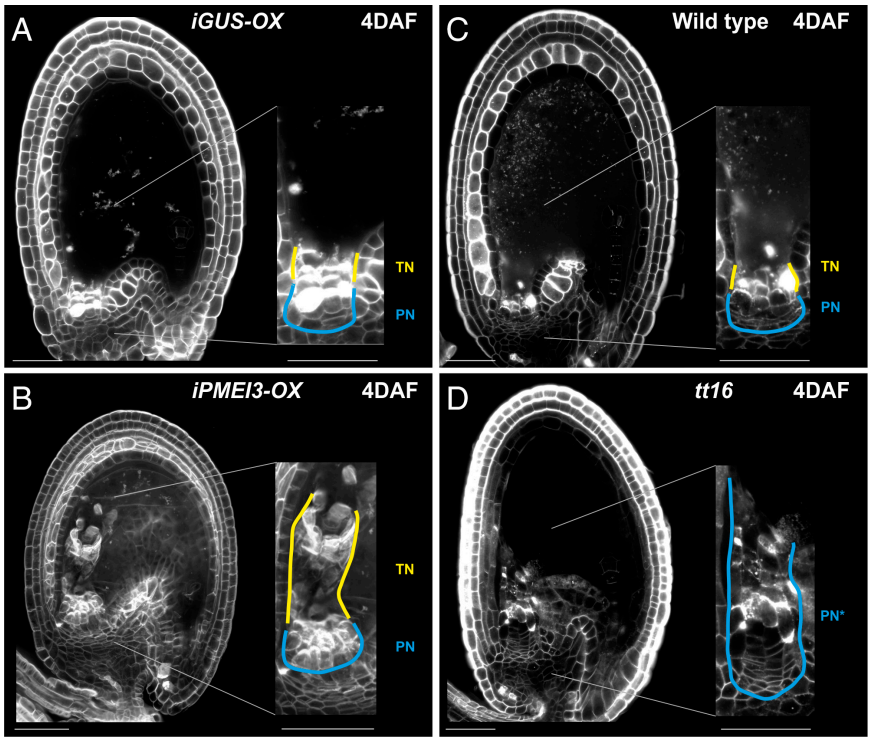

Fig. 5. Inhibition of pectin demethylesterification arrests nucellus elimination. (*A–D*) Renaissance 2200 fluorescence images of *iGUS-OX*, *iPMEI3-OX*, WT, and *tt16* seeds. DAF, days after flowering; TN, transient nucellus (yellow); PN, persistent nucellus (cyan); PN*, PN + TN not eliminated (cyan). (Scale bar, 50 μm.)

the zygotic tissues or work as apoplastic barrier. We speculated that the persistence of the TN in *tt16* seeds might lead to the formation of a hypostase-like structure in *Arabidopsis*. To test if the *tt16* nucellus produces lignin, as in the hypostase, we stained seeds with phloroglucinol, which reacts with cinnamaldehyde end-groups of lignin to give a fuchsia color. We detected phloroglucinol signal in the distal cells of the *tt16* PN*, a phenotype never observed in the WT (Fig. 7*A*). To confirm our results, we quantified lignin-derived H-, G-, and S-specific monomers using gas chromatography-mass spectrometry. We observed a higher amount of all lignin monomers in *tt16* seeds when compared to the WT (Fig. 7*B*). Finally, the *tt16* mutation led to the up-regulation of *LACCASE* and class III *PEROXIDASE* genes, known to drive lignin polymerization (Fig. 7*C*) (42). These data indicate that TT16 regulates other cell wall pathways beyond pectins and might be responsible for the development of the hypostase.

Materials and Methods

Genetic Material. The *tt16-1* allele was isolated in the Wassilewskija accession from the INRA Versailles collection (43) and then backcrossed to Columbia-0 (44, 45). *pll24-1* (SALK_049124), *pll24-2* (SALK_ 035767), *pll25-1* (SALK_031335), *pll25-2* (SALK_068375), *iPMEI5-OX* (38), and *Pro35S:gTT16-GR* (14) are in the Columbia-0 accession. *iPMEI3-OX* and *iGUS-OX* are in the Wassilewskija accession (46).

Accession Numbers. *TT16* (*AT5G23260*), *PLL24* (*AT3G24230*), *PLL25* (*AT4G13710*), *PME22* (*AT3G05620*), *PMEI3* (*AT5G20740*), *PMEI5* (*AT2G31430*).

Molecular Biology. *PLL24* 4.6 kb promoter and genomic region was PCR amplified using the gene-specific primers *PLL24F* (*5′-AGCGTGACGGATTTGGATTGA-3′*) and *PLL24R* (*5′-ACGGCAACTAAGTGCACCTGC-3′*) carrying the *attB1* (*5′-GGGGACAAGTTTGTACAAAAAAGCAGGCT-3′*) and *attB2* (*5′-GGGGACCACTTTGTACAAGAAAGCTGGGTC- 3′*) Gateway recombination sites at the 5′-ends, respectively. The PCR product was amplified with the high-fidelity Phusion DNA polymerase (Thermo Fisher Scientific), recombined into the *pDONR221* vector (BP Gateway reaction) according to the manufacturer's instructions (Thermo Fisher Scientific), sequenced, and then recombined into the *pMDC107* binary vector (47).

Transcriptomic Analyses. Libraries were prepared for Columbia-0 and *tt16-1* siliques at 0 and 2 DAF (three replicates for each genotype and time point) according to the Illumina TruSeq RNA protocol and sequenced in two lanes of a Novaseq 6000 system, yielding an average of 70 M read pairs per sample. Reads for each biological replicate were aligned independently to the *Arabidopsis thaliana* TAIR10 reference genome using hisat2 v2.1.0 (48), allowing a maximum intron length of 57,700 bp (the largest intron in the TAIR10 annotation). An average of 81.9% of the reads aligned to the reference (minimum of 77.7%). The number of reads per transcript in the TAIR10 annotation was counted with the featureCounts function in the Rsubread R package with default parameters (49). Only transcripts that presented more than 10 reads in all samples together were used in downstream analysis, leaving us with 25,053 transcripts out of the 32,678 transcripts present in the annotation.

Sample homogeneity was surveyed in R with the plotPCA function in the DEseq2 package (50) and with the PoissonDistance function in the Bioconductor PoiClaClu package (51).

GO enrichment analyses were conducted on the ShinyGO website with an FDR cutoff < 0.05 (52).

Heatmap analyses were conducted with log2-normalized counts data of three biological replicates using the Morpheus software (https://software.broadinstitute.org/morpheus). Hierarchical clustering was performed with the One Minus Pearson's Correlation metric and average linkage method.

DEX Induction. Three replicates of around 250 Columbia-0 or *35S:gTT16-GR* (14) seeds (2 DAF) per sample were harvested and immersed into a 100 μM cycloheximide (CHX) solution, vacuum treated for 10 min (breaking vacuum three times) and incubated for 20 min at room temperature. A dexamethasone (DEX) solution in ethanol was added to three Col-0 and three *35S:gTT16-GR* CHX-treated samples to a final concentration of 20 μM. The same amount of ethanol without DEX was added to the remaining three Col-0 and three *35S:gTT16-GR* CHX-treated samples. Finally, samples were vacuum treated for 10 min (breaking vacuum three times), incubated in a growth chamber for 5 h (continuous light), collected in 100 μL RNAlater (SIGMA) and frozen individually in liquid nitrogen.

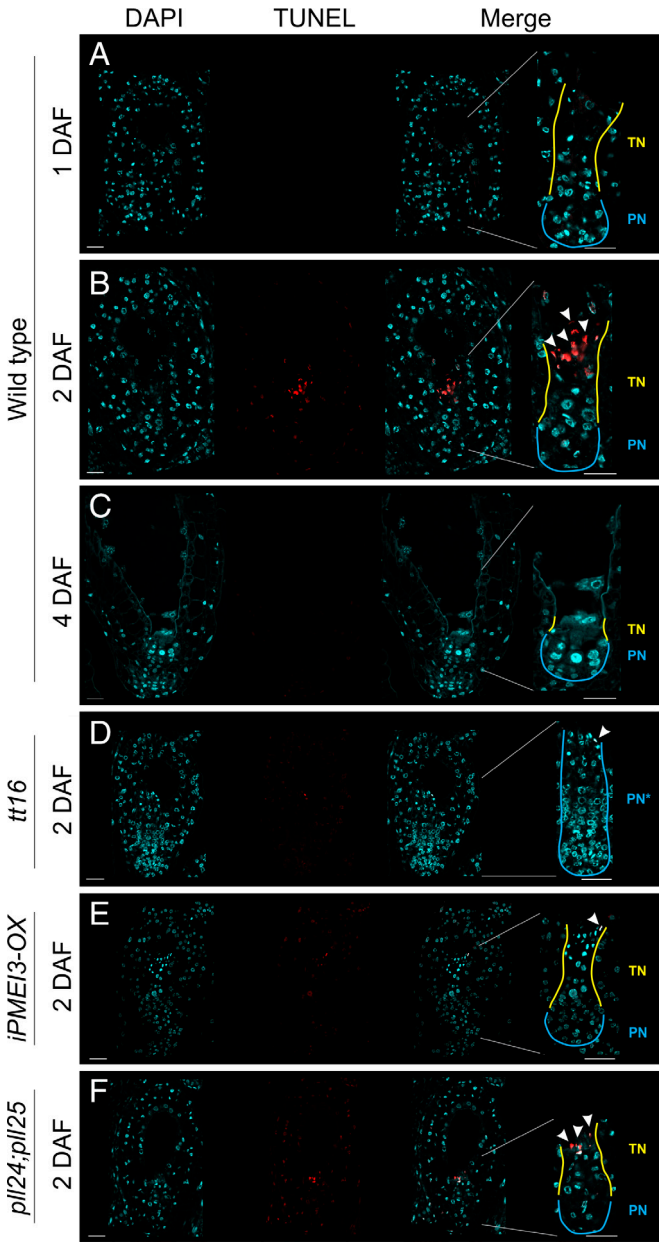

Fig. 6. Nuclear DNA fragmentation in the nucellus. (*A–F*) DAPI (in cyan) and TUNEL (in red) fluorescence images of WT, *tt16*, *iPMEI3-OX*, and *pll24;pll25* seed sections. White arrowheads indicate TUNEL positive nuclei. DAF, days after flowering; TN, transient nucellus (yellow); PN, persistent nucellus (cyan); PN*, PN + TN not eliminated (cyan). (Scale bar, 20 μm.)

Expression Analysis. For real-time RT-PCR analyses, total RNA was extracted using the mirVana miRNA isolation kit (Ambion) according to the manufacturer's instructions. The Superscript Reverse Transcriptase II kit (Invitrogen) was used to generate cDNA from 500 ng of RNA. Each cDNA sample was diluted 1:10 in water, and 4 μL of this solution was used as a template for quantitative PCR. Reactions were performed with the SYBR Green kit (Bio-Rad) on a Bio-Rad CFX real-time PCR machine according to the manufacturer's instructions. *PME22*, *PLL24*, and *PLL25* cDNAs were PCR amplified using the gene-specific primers *PME22-F* (*5′-GCAACCGTTGCTGTTTCCGG-3′*), *PME22-R* (*5′-AGAAGGCGGATTGGTCAGAA-3′*), *PLL24-F* (*5′-CTCGATCGAGGAAGCTGAAA-3′*), *PLL24-R* (*5′-GTTCACTCATGTGAATAAGG-3′*), *PLL25-F* (*5′-CTGTTCGCGGGATGATTCCA-3′*), and *PLL25R* (*5′-CTCAAAACCTTAAGAGCATC-3′*), respectively. Expression levels were normalized to the *UBIQUITIN9* expression (cDNA was PCR amplified using the gene-specific primers *UB9-F 5′-TGTAGCGCAGGACCCGTT-3′* and *UB9-R 5′-AAAGCCACCTTAGGAGGC-3′*) and were averaged from three independent biological samples. Expression levels from samples that were not treated with DEX were arbitrarily set to one.

Mass Spectrometry Analysis. Seeds (600 for each sample, n = 3) were submerged in 96% (v/v) ethanol and ground. The pellets were collected by centrifugation (13,000×*g* for 10 min) and dried in a speed vacuum concentrator at 30 °C overnight. Samples were digested with 1 U/mg dried weight of Pectobacterium carotovorum endo-Polygalacturonanase (Megazyme, Bray, Ireland) in 50 mM ammonium acetate buffer (pH 5) at 37 °C for 18 h. After digestion, samples were centrifuged at 13,000 rpm for 10 min, and 100 μL of the supernatants were transferred into vials. For mass spectrometry analysis, 10 μL of each fraction was injected into the machine. The oligosaccharides released from digestion were separated according to Voxeur et al., (34). Chromatographic separation was performed on an ACQUITY UPLC Protein BEH SEC Column (125 Å, 1.7 μm, 4.6 mm × 300 mm, Waters Corporation, Milford, MA) coupled with a guard Column BEH SEC Column (125 Å, 1.7 μm, 4.6 mm × 30 mm). Elution was performed in 50 mM ammonium formate, 0.1% formic acid at a flow rate of 0.4 mL/min, with a column oven temperature of 40 °C. The injection volume was set to 10 μL. Quantitative evaluation of cell wall fragments was conducted using an HPLC system (UltiMate 3000 RS HPLC system, Thermo Scientific, Waltham, MA) coupled to an Impact II Ultra-High Resolution Qq-Time-Of-Flight (UHR-QqTOF) spectrometer (Bruker Daltonics, Bremen, Germany) equipped with an electrospray ionization (ESI) source in negative mode. The end plate offset set voltage was 500 V, capillary voltage was 4,000 V, nebulizer pressure was 40 psi, dry gas flow was 8 L/min, and the dry temperature was set to 180 °C. The Compass 1.8 software (Bruker Daltonics) was used to acquire the data, and peak areas were integrated manually.

Inducible Gene Expression Systems. *iPMEI3-OX* and *iGUS-OX* plants were treated with ethanol as previously described (36). Nevertheless, ethanol induction of *PMEI3* tended to arrest seed development and we therefore analyzed siliques of untreated plants, which displayed a milder *PMEI3* overexpression phenotype due to the leakiness of the system. We imaged 46 *iPMEI3-OX* and 32 *iGUS-OX* seeds.

iPMEI5-OX siliques were dipped in a 100 μM estradiol (CAYMAN) or DMSO (control) solution containing 0.02% Tween-20.

GUS Assay. Harvested seeds and ovules were GUS stained as previously described (14) and analyzed by differential interference contrast microscopy with an Axioplan 2 microscope (Zeiss).

Microscopy. WT and GFP-expressing whole mount seeds were analyzed 15 min after mounting in a 100 μg·mL-1 propidium iodide, 7% sucrose solution (Weight/Volume).

For staining with Renaissance 2200, seeds were immersed in a NaOH (0.2 M), SDS (1%) solution at 37 °C for 3 h, washed three times in water, transferred to a fresh bleach solution (2%) for 10 min to remove precipitated tannins, washed five times, and then mounted in Renaissance 2200 solution diluted 100 times with water.

Immunolabeling and CBM3 histochemical analyses were conducted as previously described (31). We examined more than three slides, each carrying 32 to 100 sections of both WT and mutant samples derived from more than five siliques, per experiment.

For TUNEL experiments, we used the In Situ Cell Death Detection Kit, TMR red (Roche) and followed the manufacturer's instructions.

Samples were imaged by confocal laser scanning microscopy (Leica SP8 and Zeiss LSM 710) keeping conditions uniform between samples to allow cross-comparisons.

The GFP and PI mean fluorescence intensity was quantified using the Fiji software (53).

Quantitative Analysis of Immunolabeling Experiments. The multisegment linear region of interest was drawn manually using Fiji with a line thickness spanning the entire nucellus. Subsequent analyses were carried out in Matlab, utilizing custom-written scripts available on GitHub. The raw data comprised the total intensity (summed over the line thickness) for two imaging channels at specific points along the line segment. The imaged seeds exhibited variability in size due to natural differences in developmental stages. To consolidate the data, we assumed that seeds preserved the proportion between persistent and transient nucellus regardless of their size. Consequently, we interpolated the data using the same number of query points for all seeds, employing Matlab's built-in function interp1, and the interpolation grid was generated using the linspace function.

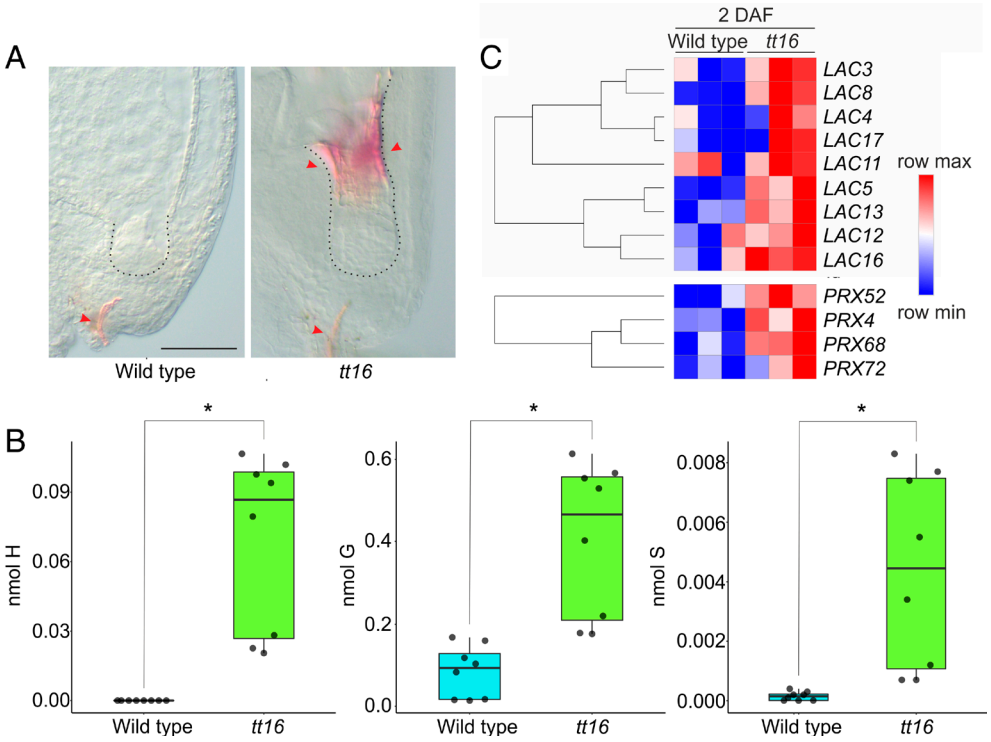

Fig. 7. *tt16* mutation promotes lignin formation. (*A*) Differential interference contrast microscopy images of seeds (4 DAF) stained with phloroglucinol to detect lignin. The contour of the nucellus is outlined by a dotted line. Arrowheads indicate phloroglucinol staining in the xylem and in the nucellus. (Scale bar, 50 μm.) (*B*) Quantification of lignin-derived H, G, and S specific monomers using gas chromatography-mass spectrometry. Asterisks indicate statistically significant difference between WT and *tt16* (Student's *t* test, $P < 0.05$). Error bars indicate SD. (*C*) Heatmaps showing the expression of *LACCASES* (*LAC*) and class III *PEROXIDASES* (*PRX*) genes up-regulated in *tt16* seeds at 2 DAF, when compared to the WT.

Finally, the data were normalized as follows: IN-LM20 = ILM20/(ILM20 + I2F4), IN-2F4 = I2F4/(ILM20 + I2F4), where ILM20 and I2F4 represent the staining intensity of methylated and demethylated homogalacturonans, respectively. IN-LM20 and IN-2F4 are presented as averages (n = 10 seeds per genotype, selected from three slides), ± the SEM. Comparison of IN-LM20 and IN-2F4 data between WT and *tt16* was performed at each query point using the Wilcoxon rank test at a confidence level of 0.05.

Lignin Analyses. Seeds were stained with phloroglucinol, mounted in chloral hydrate, and imaged by differential interference contrast microscopy.

For lignin quantification experiments, 30 seeds at bending torpedo embryo stage were kept in 1 mL thioacidolysis reagent at 100 °C for 4 h, together with 2.59 μg C^{21} internal standard. The lignin-derived H-, G-, or S-specific monomers (recovered aa pairs of erythro/threo diastereoisomers) were then extracted from the reaction medium, silylated (by BSTFA) and analyzed as their trimethysilylated derivatives by gas chromatography–mass spectrometry (GC–MS). The GC–MS analysis of the H, G, and S monomers specifically released from lignins was conducted using ion chromatograms respectively reconstructed at m/z 239, 269, and 299, as compared to the internal standard (evaluated on the ion chromatogram reconstructed at m/z 57 + 71 + 85). As the analyses were performed on trace amounts, a blank assay was performed to check that the H, G, and S detected monomers actually originated from the seed samples.

Bioinformatic Analyses. PLL24 protein structure was modeled using AlphaFold (54). Multiple sequence alignments were performed using Muscle (55) and visualized using BioEdit (56).

Discussion

Nucellus elimination was instrumental to seed evolution as it allowed the growth of female gametophyte and endosperm inside the maternal sporophyte. Compared to most other cell death programs, cell elimination appears to dismantle the cell wall, a unique process that was not fully addressed at the molecular level. Here, we show that demethylesterification of the cell wall homogalacturonan (HG) initiates the elimination of the nucellus in *Arabidopsis*.

Dismantling the Cell Wall Starting from Its Pectic Component. The cell wall is a unique component of plant cells that provides strength, rigidity, and protection, through its chemical composition that is hard to break down (21, 57). Indeed, most cell death programs do not eliminate the cell wall but only the intracellular content (18, 39). The nucellus tissue, with few other examples (18), constitutes an exception to such a rule as its most distal cell walls are dismantled to reorganize the internal space of the seed and make room for the growth of the endosperm. This process has been already described in a number of species, including *Arabidopsis*, but only at the morphological level (5). Here, we identify pectin degradation as the gate to nucellus elimination by analyzing transcriptomic data obtained across fertilization. Our analysis revealed, indeed, a significant enrichment in the GO term pectin metabolic process among genes differentially expressed right after fertilization. The list of functions attributed to pectins has been expanding in recent years. Originally considered important for intercellular adhesion because of their abundance in the middle lamella, pectins have been now shown to be involved in cell fate specification, morphogenesis, intercellular communication, and environmental sensing (58). HG is secreted into the cell wall as methylesterified polymer (26) and then subjected to demethylesterification via the action of wall-bound pectin methylesterases (PMEs), which ultimately affect the mechanical properties of the cell wall (27). PMEs produce free carboxyl groups that can interact with Ca^{2+} to create a pectic gel, thus increasing cell wall stiffness. Alternatively, low methylesterification of HG is recognized as cleavage site by PECTATE LYASE (PL) or POLYGALACTURONASE (PG)

enzymes that trigger HG depolymerization, thereby promoting cell wall loosening. The rapid transcriptional up-regulation of the pectin-degrading machinery observed after fertilization in the TN suggested that the cell walls are deprived of their pectic component to proceed further into cell elimination. Immunolabeling analyses confirmed that HG is preferentially low methylesterified in the TN after fertilization, when clear morphological signs of nucellus elimination are not yet visible. HG demethylesterification is therefore the first known hallmark of nucellus elimination and is rapidly followed by the detection of crystalline cellulose. We hypothesize that cellulose is accessible only after HG degradation in nondividing or expanding cells. This scenario was confirmed by detecting PECTATE LYASE LIKE 24 (PLL24) in the TN during its elimination. Furthermore, we showed that the amount of degradable HG was higher in two independent *pll24;25* mutant lines, when compared to the WT. These data suggest that PLL24 and PLL25 actively degrade HG in the TN, exposing other cell wall polymers, such as cellulose, to possible further degradation.

Modification of the pectin status in the TN is regulated by the TT16 transcription factor, which promotes cell elimination. *tt16* seeds displayed preferentially high methylesterified HG in the distal nucellus and down-regulation of *PLL24* expression, a pattern diametrically opposed to what observed in the WT. Furthermore, our TT16-GR induction analyses indicate that *PLL24* and *PME22* are immediate targets of TT16. We therefore suggest that TT16 might promote TN elimination by inducing HG demethylesterification and degradation. Nevertheless, TT16 also influences the lignin pathway, suggesting that its role in cell wall modification extends beyond pectins. Alternatively, TT16 might influence lignification indirectly via its effects on pectin modification. Certain pectin side-chain decorations can be feruloylated, offering a potential mechanistic bridge between pectin structure and secondary-wall lignification, as lignin polymers are known to form bonds with ferulate residues (59). In line with results obtained in the *tt16* mutant, the PN of WT seeds showed a higher level of HG methylesterification, when compared to the TN, which might guarantee its survival. In support of this hypothesis, the inhibition of HG demethylesterification by *PMEI3* overexpression arrested the elimination of the TN. This result clearly shows a causal effect of cell wall modification on the development of the nucellus. Our model relates to studies conducted in cereals. In barley ovules, HG in the distal nucellus has been shown to be low methylesterified and interpreted as responsible for keeping the cells more rigid and less prone to degradation (60). In light of what presented here, we believe that this hypothesis should be revised in favor of a role of HG demethylesterification in initiating cell wall degradation. Consistent with our results, Qin Sun et al. showed that the maize EXPANSIN B15, a protein responsible for cell wall loosening, promotes the process of nucellus elimination (61). We speculate that expansins might facilitate the work of PME and PLL enzymes by relaxing the cell wall. Both articles describe an effect of nucellus development on grain size, thus opening the way to novel approaches for yield-improvement. Our results might contribute to the design of lines showing a faster or slower elimination of the nucellus by regulating the HG esterification status.

Evolving a Seed by Modifying the Cell Wall? The elimination of the nucellus marked the evolution of the seed habit as it allowed the growth of the spores inside the sporophyte instead of releasing them. The same mechanism was exploited by angiosperms to evolve endospermic seeds, such as *Arabidopsis* and cereals, which favor the growth of the endosperm at the expense of the nucellus. Here, we show that the process of pectin demethylesterification is necessary to trigger the dismantling of the nucellus cell walls. Therefore, we speculate that a change in the pectin status might have started such evolutionary breakthroughs that had a profound impact on our society. However, a more in-depth phylogenetic analysis is necessary to address this hypothesis.

A similar set of events has been described during pathogen attacks. The first step in the infection of plant cells by necrotrophic fungi is indeed the demethylesterification and degradation of pectins to improve cell wall accessibility to other degrading enzymes and achieve a successful penetration (62). Another parallel can be drawn between the elimination of the nucellus and the softening of the endosperm during embryo growth. In *Arabidopsis*, the bHLH-type transcription factor ZHOUPI (ZOU), similarly to TT16, promotes weakening of the endosperm cell walls by regulating the activity of a series of cell wall-modifying enzymes (63, 64). In *zou* mutant seeds, the (1-5)-α-L-arabinan epitopes, which might be associated with rhamnogalacturonan-1 pectins, were more abundant and persistent than in the WT. These data suggest that ZOU might soften the endosperm cell wall by modifying pectins. Finally, the clearance of dying cells in animals is undertaken by phagocytes, which engulf and digest cell corpse and extracellular matrix (65). Despite their profound differences, the plant cell wall and the animal extracellular matrix are both composed of polysaccharides and proteins (66). Similar to HG in plants, hyaluronic acid (HA) polymers are nonprotein polysaccharides within the mammalian extracellular matrix with pivotal structural and signaling roles in programmed cell death, cellular mobility, and the regulation of cancer (67). A number of studies have associated changes in the molecular weight of HA polymers with apoptosis and phagocytic elimination in cancer cells (67). The striking convergence in both the structure and function of HA and HG emphasizes the crucial contribution of sugar-derived polymers to the emergence of multicellular organisms.

Finally, *tt16* seeds exhibited a lignified persistent nucellus, resembling the hypostase. While the function of the hypostase is not yet fully understood, it has been speculated that it mechanically regulates endosperm growth and forms an apoplastic barrier (5, 41). In *tt16* mutant seeds, the nucellus affects both endosperm development and sugar transport (14, 15), suggesting that TT16 expression or activity in the chalazal nucellus may have played a role in the evolution or loss of the hypostase in different species. This hypothesis should be tested in monocotyledonous seeds that possess a hypostase.

Dying While the Cell Wall Is Eliminated. The elimination of the cell wall might lead to the death of the TN nucellus cells without invoking any intracellular cell death program. Such a scenario seemed to be suggested by transmitted electron microscope images showing cell corpses released in the apoplast during nucellus elimination (14). Nevertheless, we detected DNA fragmentation in the nuclei of TN cells after HG demethylesterification but before cell wall dismantling. Nuclear DNA degradation has been detected in a number of developmental cell death programs (39, 68), thus suggesting that the TN undergoes programmed cell death as well as cell wall degradation. Combining both processes might allow the TN to predigest cellular material before the collapse of the cell walls. Further processing of the cell corpses might then continue in the apoplast.

TUNEL experiments in *tt16* seeds showed that only a few distal cells of the TN nucellus undergo DNA fragmentation while most of the nucellus expand in apparent coordination with the rest of the maternal tissues. These data suggest that PCD and cell wall degradation are either independent processes coregulated by TT16 or interdependent pathways downstream of TT16. The reduced TUNEL signal detected in *iPMEI3-OX* seeds supports the latter

scenario, suggesting that TT16 promotes HG demethylesterification, which in turn triggers DNA fragmentation. During the elimination of the endosperm cells, ZOU promotes weakening of the cell walls while NAC transcription factors induce PCD (63, 64, 69). In the *zou* mutant, the endosperm displays intact cell walls but expression of *NAC* and PCD marker genes, despite being delayed. These data indicate that the ZOU transcription factor is principally responsible for the softening of the cell wall and not PCD. TT16 and ZOU might therefore regulate cell elimination in a similar fashion, with PCD in *tt16* seeds being substantially delayed. Further experiments are necessary to identify the genes responsible for PCD in the nucellus to test such hypotheses.

Data, Materials, and Software Availability. The transcritomic raw data are available here: https://www.ncbi.nlm.nih.gov/bioproject/PRJNA1111692 (70). All other data are included in the article and/or supporting information.

ACKNOWLEDGMENTS. We thank Gwyneth Ingram, Herman Höfte, Samantha Vernhettes, and members of their groups for helpful discussions, Lothar Kalmbach for the iPMEI5-OX line, and the Observatoire du Végétal for plant culture, access to imaging and mass spectrometry facilities, and assistance. The project was financially supported by the Agence Nationale de la Recherche (ANR) under grant ANR-20-CE20-0018 (*Cleanse*), the LabEx Saclay Plant Sciences (SPS) under Grant ANR-10-LABX-0040-SPS, the SPS doctoral fellowship *Cell Wall Elimination in Seeds*, and the Italian Ministry of University and Research within the framework of the programme PRIN 2022 a scorrimento–Grant No.: 2022ASSR9R-CUP: H53C24001230006.

1. Y. Huang *et al.*, Revisiting the female germline cell development. *Front. Plant Sci.* **15**, 1525729 (2024).
2. J. A. Banks, *Selaginella* and 400 million years of separation. *Annu. Rev. Plant Biol.* **60**, 223–238 (2009).
3. J. Pettitt, Heterospory and the origin of the seed habit. *Biol. Rev.* **45**, 401–415 (1970).
4. E. Magnani, Seed evolution. A "simpler" story. *Trends Plant Sci.* **23**, 654–656 (2018).
5. J. Lu, E. Magnani, Seed tissue and nutrient partitioning, a case for the nucellus. *Plant Reprod.* **31**, 309–317 (2018).
6. S. Nayar, R. Sharma, A. K. Tyagi, S. Kapoor, Functional delineation of rice MADS29 reveals its role in embryo and endosperm development by affecting hormone homeostasis. *J. Exp. Bot.* **64**, 4239–4253 (2013).
7. L. L. Yin, H. W. Xue, The MADS29 transcription factor regulates the degradation of the nucellus and the nucellar projection during rice seed development. *Plant Cell* **24**, 1049–1065 (2012).
8. W. W. Mayne, Mysore coffee. *Kip. Sta. Bull* **16**, 6 (1937).
9. L. C. Alves *et al.*, Differentially accumulated proteins in *Coffea arabica* seeds during perisperm tissue development and their relationship to coffee grain size. *J. Agric. Food Chem.* **64**, 1635–1647 (2016).
10. S. K. Floyd, W. E. Friedman, Evolution of endosperm developmental patterns among basal flowering plants. *Int. J. Plant Sci.* **161**, S57–S81 (2000).
11. J. Wang *et al.*, Auxin efflux controls orderly nucellar degeneration and expansion of the female gametophyte in *Arabidopsis*. *New Phytol.* **230**, 2261–2274 (2021).
12. W. C. Yang, D. Ye, J. Xu, V. Sundaresan, The SPOROCYTELESS gene of *Arabidopsis* is required for initiation of sporogenesis and encodes a novel nuclear protein. *Genes Dev.* **13**, 2108–2117 (1999).
13. U. Schiefthaler *et al.*, Molecular analysis of NOZZLE, a gene involved in pattern formation and early sporogenesis during sex organ development in *Arabidopsis thaliana*. *Proc. Natl. Acad. Sci. U.S.A.* **96**, 11664–11669 (1999).
14. W. Xu *et al.*, Endosperm and nucellus develop antagonistically in *Arabidopsis* seeds. *Plant Cell* **28**, 1343–1360 (2016).
15. J. Lu *et al.*, The nucellus: Between cell elimination and sugar transport. *Plant Physiol.* **185**, 478–490 (2021).
16. X. Yang *et al.*, *MADS31* supports female germline development by repressing the post-fertilization programme in cereal ovules. *Nat. Plants* **11**, 543–560 (2025).
17. X. Yang *et al.*, Live and let die–The B(sister) MADS-box gene *OsMADS29* controls the degeneration of cells in maternal tissues during seed development of rice (*Oryza sativa*). *PLoS One* **7**, e51435 (2012).
18. G. C. Ingram, Dying to live: Cell elimination as a developmental strategy in angiosperm seeds. *J. Exp. Bot.* **68**, 785–796 (2017).
19. F. Xie, H. Vahldick, Z. Lin, M. K. Nowack, Killing me softly–Programmed cell death in plant reproduction from sporogenesis to fertilization. *Curr. Opin. Plant Biol.* **69**, 102271 (2022).
20. D. Delmer, R. A. Dixon, K. Keegstra, D. Mohnen, The plant cell wall-dynamic, strong, and adaptable–Is a natural shapeshifter. *Plant Cell* **36**, 1257–1311 (2024).
21. Z. A. Popper *et al.*, Evolution and diversity of plant cell walls: From algae to flowering plants. *Annu. Rev. Plant Biol.* **62**, 567–590 (2011).
22. M. F. Belmonte *et al.*, Comprehensive developmental profiles of gene activity in regions and subregions of the *Arabidopsis* seed. *Proc. Natl. Acad. Sci. U.S.A.* **110**, E435–E444 (2013).
23. D. D. Figueiredo, R. A. Batista, P. J. Roszak, L. Hennig, C. Kohler, Auxin production in the endosperm drives seed coat development in *Arabidopsis*. *eLife* **5**, e20542 (2016).
24. M. Schena, A. M. Lloyd, R. W. Davis, A steroid-inducible gene expression system for plant cells. *Proc. Natl. Acad. Sci. U.S.A.* **88**, 10421–10425 (1991).
25. L. Sun, S. van Nocker, Analysis of promoter activity of members of the pectate lyase-like (PLL) gene family in cell separation in *Arabidopsis*. *BMC Plant Biol.* **10**, 152 (2010).
26. D. Mohnen, Pectin structure and biosynthesis. *Curr. Opin. Plant Biol.* **11**, 266–277 (2008).
27. D. Qiu, S. Xu, Y. Wang, M. Zhou, L. Hong, Primary cell wall modifying proteins regulate wall mechanics to steer plant morphogenesis. *Front. Plant Sci.* **12**, 751372 (2021).
28. C. M. Rounds, E. Lubeck, P. K. Hepler, L. J. Winship, Propidium iodide competes with Ca(2+) to label pectin in pollen tubes and *Arabidopsis* root hairs. *Plant Physiol.* **157**, 175–187 (2011).
29. F. Liners, J. J. Letesson, C. Didembourg, P. Van Cutsem, Monoclonal antibodies against pectin: Recognition of a conformation induced by calcium. *Plant Physiol.* **91**, 1419–1424 (1989).
30. Y. Verhertbruggen, S. E. Marcus, A. Haeger, J. J. Ordaz-Ortiz, J. P. Knox, An extended set of monoclonal antibodies to pectic homogalacturonan. *Carbohydr. Res.* **344**, 1858–1862 (2009).
31. K. T. Haas, M. Rivière, R. Wightman, A. Peaucelle, Multitarget immunohistochemistry for confocal and super-resolution imaging of plant cell wall polysaccharides. *Bio-protocol* **10**, e3783 (2020).
32. K. Thorne, B. Urbanowicz, M. Hahn, "Plant cell wall glycan-directed monoclonal antibodies" in *Plant Cell Walls* (2023), pp. 206–236.
33. E. W. Czerwinski, T. Midoro-Horiuti, M. A. White, E. G. Brooks, R. M. Goldblum, Crystal structure of Jun a 1, the major cedar pollen allergen from *Juniperus ashei*, reveals a parallel beta-helical core. *J. Biol. Chem.* **280**, 3740–3746 (2005).
34. A. Voxeur *et al.*, Oligogalacturonide production upon. *Proc. Natl. Acad. Sci. U.S.A.* **116**, 19743–19752 (2019).
35. A. Paterlini *et al.*, Enzymatic fingerprinting reveals specific xyloglucan and pectin signatures in the cell wall purified with primary plasmodesmata. *Front. Plant Sci.* **13**, 1020506 (2022).
36. K. T. Haas, R. Wightman, E. M. Meyerowitz, A. Peaucelle, Pectin homogalacturonan nanofilament expansion drives morphogenesis in plant epidermal cells. *Science* **367**, 1003–1007 (2020).
37. F. Xu *et al.*, Biochemical characterization of Pectin Methylesterase Inhibitor 3 from *Arabidopsis thaliana*. *Cell Surf.* **8**, 100080 (2022).
38. L. Kalmbach *et al.*, Putative pectate lyase PLL12 and callose deposition through polar CALS7 are necessary for long-distance phloem transport in *Arabidopsis*. *Curr. Biol.* **33**, 926–939.e9 (2023).
39. T. Van Hautegem, A. J. Waters, J. Goodrich, M. K. Nowack, Only in dying, life: Programmed cell death during plant development. *Trends Plant Sci.* **20**, 102–113 (2015).
40. Y. Gavrieli, Y. Sherman, S. A. Ben-Sasson, Identification of programmed cell death in situ via specific labeling of nuclear DNA fragmentation. *J. Cell Biol.* **119**, 493–501 (1992).
41. P. J. Rudall, The nucellus and chalaza in monocotyledons: Structure and systematics. *Bot. Rev.* **63**, 140–181 (1997).
42. W. Boerjan, J. Ralph, M. Baucher, Lignin biosynthesis. *Annu. Rev. Plant Biol.* **54**, 519–546 (2003).
43. N. Bechtold, G. Pelletier, In planta *Agrobacterium*-mediated transformation of adult *Arabidopsis thaliana* plants by vacuum infiltration. *Methods Mol. Biol.* **82**, 259–266 (1998).
44. O. Coen *et al.*, Developmental patterning of the sub-epidermal integument cell layer in *Arabidopsis* seeds. *Development* **144**, 1490–1497 (2017).
45. N. Nesi *et al.*, The TRANSPARENT TESTA16 locus encodes the ARABIDOPSIS BSISTER MADS domain protein and is required for proper development and pigmentation of the seed coat. *Plant Cell* **14**, 2463–2479 (2002).
46. A. Peaucelle, R. Wightman, K. T. Haas, Multicolor 3D-dSTORM reveals native-state ultrastructure of polysaccharides' network during plant cell wall assembly. *iScience* **23**, 101862 (2020).
47. M. D. Curtis, U. Grossniklaus, A gateway cloning vector set for high-throughput functional analysis of genes in planta. *Plant Physiol.* **133**, 462–469 (2003).
48. D. Kim, B. Langmead, S. L. Salzberg, HISAT: A fast spliced aligner with low memory requirements. *Nat. Methods* **12**, 357–360 (2015).
49. Y. Liao, G. K. Smyth, W. Shi, The R package Rsubread is easier, faster, cheaper and better for alignment and quantification of RNA sequencing reads. *Nucleic Acids Res.* **47**, e47 (2019).
50. M. I. Love, W. Huber, S. Anders, Moderated estimation of fold change and dispersion for RNA-seq data with DESeq2. *Genome Biol.* **15**, 550 (2014).
51. W. Dm, Classification and clustering of sequencing data using a Poisson model. *Ann. Appl. Stat.* **5**, 2493–2518 (2011).
52. S. X. Ge, D. Jung, R. Yao, ShinyGO: A graphical gene-set enrichment tool for animals and plants. *Bioinformatics* **36**, 2628–2629 (2020).
53. J. Schindelin *et al.*, Fiji: An open-source platform for biological-image analysis. *Nat. Methods* **9**, 676–682 (2012).
54. J. Jumper *et al.*, Highly accurate protein structure prediction with AlphaFold. *Nature* **596**, 583–589 (2021).
55. R. C. Edgar, MUSCLE: Multiple sequence alignment with high accuracy and high throughput. *Nucleic Acids Res.* **32**, 1792–1797 (2004).
56. T. A. Hall, BioEdit: A user-friendly biological sequence alignment editor and analysis program for Windows 95/98/NT. *Nucleic Acids Symp. Ser.* **41**, 95–98 (1999).
57. F. Sc, *The Growing Plant Cell Wall: Chemical and Metabolic Analysis* (Longman Scientific & Technical, Harlow, UK, 1988), pp. 103–185.
58. Y. Shin, A. Chane, M. Jung, Y. Lee, Recent advances in understanding the roles of pectin as an active participant in plant signaling networks. *Plants (Basel)* **10**, 1712 (2021).
59. C. T. Anderson, J. Pelloux, The dynamics, degradation, and afterlives of pectins: Influences on cell wall assembly and structure, plant development and physiology, agronomy, and biotechnology. *Annu. Rev. Plant Biol.* **76**, 85–113 (2025).
60. X. Yang *et al.*, Ovule cell wall composition is a maternal determinant of grain size in barley. *New Phytol.* **237**, 2136–2147 (2023).
61. Q. Sun *et al.*, A NAC-EXPANSIN module enhances maize kernel size by controlling nucellus elimination. *Nat. Commun.* **13**, 5708 (2022).
62. C. P. Kubicek, T. L. Starr, N. L. Glass, Plant cell wall-degrading enzymes and their secretion in plant-pathogenic fungi. *Annu. Rev. Phytopathol.* **52**, 427–451 (2014).
63. S. Yang *et al.*, The endosperm-specific ZHOUPI gene of *Arabidopsis thaliana* regulates endosperm breakdown and embryonic epidermal development. *Development* **135**, 3501–3509 (2008).
64. C. Fourquin *et al.*, Mechanical stress mediated by both endosperm softening and embryo growth underlies endosperm elimination in *Arabidopsis* seeds. *Development* **143**, 3300–3305 (2016).
65. A. M. Fond, K. S. Ravichandran, Clearance of dying cells by phagocytes: Mechanisms and implications for disease pathogenesis. *Adv. Exp. Med. Biol.* **930**, 25–49 (2016).
66. L. Stavolone, V. Lionetti, Extracellular matrix in plants and animals: Hooks and locks for viruses. *Front. Microbiol.* **8**, 1760 (2017).

67. M. Bhattacharyya, H. Jariyal, A. Srivastava, Hyaluronic acid: More than a carrier, having an overpowering extracellular and intracellular impact on cancer. *Carbohydr. Polym.* **317**, 121081 (2023).
68. D. Latrasse, M. Benhamed, C. Bergounioux, C. Raynaud, M. Delarue, Plant programmed cell death from a chromatin point of view. *J. Exp. Bot.* **67**, 5887–5900 (2016).
69. N. M. Doll *et al.*, Endosperm cell death promoted by NAC transcription factors facilitates embryo invasion in *Arabidopsis*. *Curr. Biol.* **33**, 3785–3795.e6 (2023).
70. W. Xu, J. M. Jiménez-Gómez, E. Magnani, Transcriptomic profiling of Arabidopsis wild type and transparent testa 16 seeds across fertilization. NCBI BioProject. https://www.ncbi.nlm.nih.gov/bioproject/PRJNA1111692. Deposited 15 May 2024.